SPACE WEATHER, VOL. 5, S08001, doi:10.1029/2007SW000314, 2007

A tool to improve space weather forecasts: Kilometric radio emissions from Wind/WAVES

H. Cremades,[1] O. C. St. Cyr,[2] and M. L. Kaiser[2]

Received 18 January 2007; revised 14 March 2007; accepted 25 March 2007; published 11 August 2007.

[1] For decades, space environment forecasters have used the appearance of metric Type II radio emission as a proxy for eruptions in the solar corona. The drift rate of these near-Sun emissions is often turned into a speed, commonly assumed to be that of an MHD shock. However, their utility to forecast shock arrival times has not proved to be conclusive. Metric emissions can be detected by ground-based antennae, while lower-frequency components of these slowly drifting emissions can also be tracked by spacecraft in interplanetary space, as far down in frequency as that of the local plasma frequency. For a spacecraft at L1, this corresponds to about 25 kHz, or an electron density of about 7 cm^{-3} in the ambient solar wind. Here we report a recent study that aims to improve the predictions of shock arrival time at L1 by means of the low-frequency emissions detected by WIND/WAVES. This technique, implemented on an extensive sample of hectometric and kilometric type II radio bursts, has yielded promising results.

Citation: Cremades, H., O. C. St. Cyr, and M. L. Kaiser (2007), A tool to improve space weather forecasts: Kilometric radio emissions from Wind/WAVES, *Space Weather*, *5*, S08001, doi:10.1029/2007SW000314.

1. Introduction

[2] Space weather is predominantly governed by solar activity, particularly by solar eruptions. Undoubtedly, the most impressive types of eruptions are coronal mass ejections (CMEs). As they travel through interplanetary space at speeds in excess of 2000 km s^{-1}, they carry vast amounts of plasma and magnetic fields and can drive extensive MHD shocks. These shocks accelerate energetic particles and produce storm sudden commencement at Earth. The shocks precede the strongest magnetic fields that make up the CME, which may interact with Earth's magnetosphere, ultimately triggering a geomagnetic storm. The most intense storms are produced by the fastest CMEs, which carry with them the strongest interplanetary magnetic fields. Furthermore, most of the fastest CMEs drive shocks that are detected by spacecraft at L1 [*Sheeley et al.*, 1985; *Cane et al.*, 1987]. Therefore it is of utmost importance in the space weather field to find ways of forecasting the arrival time of such phenomenon. A number of models [e.g., *Schwenn et al.*, 2001; *Gopalswamy et al.*, 2001a, 2001b] intend to forecast the travel time of a CME to Earth on the basis of white-light CME observations, yielding predictions with rms errors of 9.2 hours to 10.6 hours [*Smith et al.*, 2003].

[3] After they have left the field of view of coronagraphs, there are only a few ways to track CMEs. Recent attempts to detect CMEs in Lyman-alpha using SWAN on SOHO were not successful [*Mays et al.*, 2007]. Latest results from the Solar Mass Ejection Imager (SMEI) [e.g., *Howard et al.*, 2006] show that at least some CMEs can be tracked in white light far away from the Sun. Ground-based Interplanetary Scintillation (IPS) measurements have also had some success tracking disturbances after they have left the Sun [e.g., *Manoharan*, 2006]. New results from the Heliospheric Imager on the STEREO mission indicate another apparent successful method to image CMEs [*Howard et al.*, 2007].

[4] When a shock travels outward from the solar corona, it excites electrons which in turn produce an emission at the local plasma frequency ($f = 9\sqrt{n_e}$) and its first harmonic. As the shock encounters more rarefied regions, the local plasma frequency decreases giving rise to a slow-drift or type II radio burst. These interplanetary emissions usually start at frequencies below 150 MHz, when the disturbance is just few solar radii away from the Sun. They may extend down to the kilometric domain, slowly drifting to lower frequencies all the way to 1 AU, where the local plasma frequency of the solar wind is ~25 kHz (see Figure 1 for examples). Since Earth's ionosphere blocks radio signals below ~10 MHz, the only way to detect the longer-wavelength emissions is by means of instruments in interplanetary space. Nowadays, that is the task of the Wind/WAVES experiment [*Bougeret et al.*, 1995] and of the recently launched STEREO/WAVES [*Bougeret et al.*, 2007].

[1]NASA Postdoctoral Program, NASA Goddard Space Flight Center, Greenbelt, Maryland, USA.
[2]NASA Goddard Space Flight Center, Greenbelt, Maryland, USA.

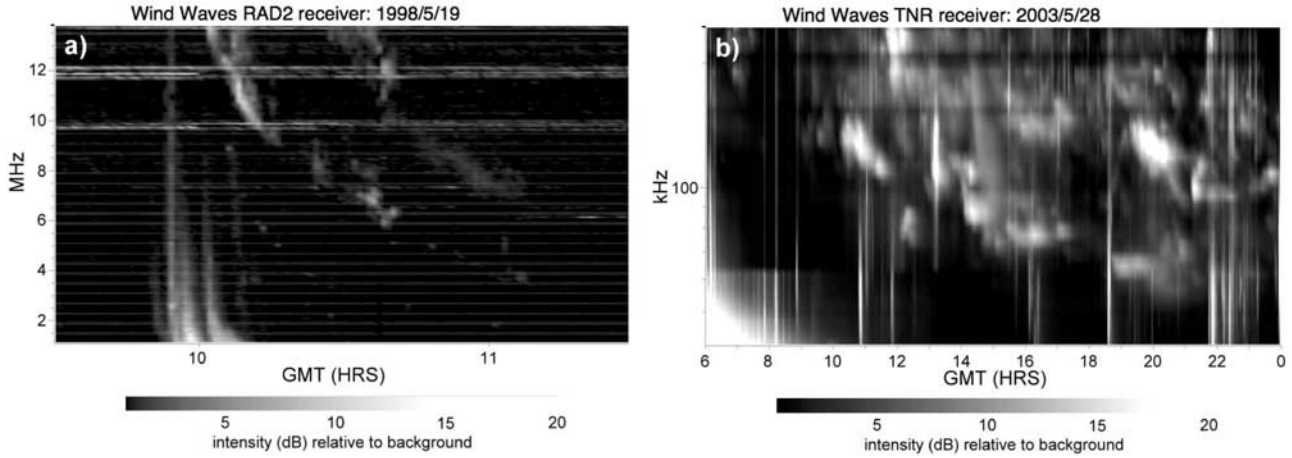

Figure 1. Examples of type II radio bursts registered by the Wind/WAVES experiment, showing (a) a metric type II burst and (b) a hectometric/kilometric burst. Note the difference in the vertical scales: Figure 1a is in the linear frequency domain, while Figure 1b is in logarithmic scale.

[5] Previous investigations of type II radio bursts have allowed the development of models toward the prediction of CME shock arrival times at Earth. In particular, these models rely on type II radio bursts occurring in the metric domain to obtain information on the shock kinematics. The most prominent of these models include Shock Time of Arrival (STOA) [*Dryer and Smart*, 1984], Interplanetary Shock Propagation Model (ISPM) [*Smith and Dryer*, 1995], and Hakamada-Akasofu-Fry v.2 (HAFv.2) [*Fry et al.*, 2001]. Several studies have compared the degree of success of these models [*McKenna-Lawlor et al.*, 2002; *Cho et al.*, 2003; *Fry et al.*, 2003; *Smith et al.*, 2003; *McKenna-Lawlor et al.*, 2006], finding an average prediction error of ~11 hours. Moreover, there are disparate opinions on the validity of these models, since there is some debate on the nature of the mechanism that generates metric type II radio bursts. Studies on the location of the metric type II emission reveal that it occurs at the rear of the leading edge of CMEs [e.g., *Gary et al.*, 1984; *Pick*, 1999]. *Gopalswamy et al.* [2001a, 2001b] studied the correspondence between 44 metric type II events and 46 shocks detected in situ and found that 93% of the metric emissions did not have in situ IP events and 80% of IP events had no metric counterparts. *Claßen and Aurass* [2002] found big disparities between the speeds from drift rates of 63 metric type II bursts and those of their associated CMEs and propose three different scenarios for metric type II generation. *Fry et al.* [2003] also noted that apparent CME speeds measured in coronagraph's observations cannot be decisively related to shock speeds measured above solar flare sites. *Cane and Erickson* [2005] found no clear example of a metric type II burst that extends down in frequency without disruption to turn into a hectometric/kilometric type II event, implying that metric type II bursts are probably not caused by shocks driven in front of CMEs.

[6] Here we present recent work aimed at improving the present errors in forecasting shock arrival times, while at the same time avoiding the inconsistencies between metric type II radio bursts and CME shocks. We have focused on kilometric type II (kmTII) radio bursts observed over the past decade by Wind/WAVES. There have been previous studies on emissions at these low frequencies, but they are focused on specific events [*Reiner et al.*, 1998a; *Dulk et al.*, 1999; *Leblanc et al.*, 2001]. To our knowledge, it is the first time that this approach has been applied on a statistically significant sample of kmTII radio emissions. The details on the selection of the studied events are presented in the following section. The procedure applied to obtain CME shock arrival time from the drift rates of kmTIIs is described in section 3. The arrival time of the shocks temporally associated with the studied kmTIIs is compared with that deduced from the kmTIIs drift rates and presented in section 4.

2. Data and Event Selection

[7] The radio data analyzed in this report were acquired by the WAVES experiment on the Wind spacecraft [*Bougeret et al.*, 1995]. WAVES measures radio emissions in three different spectral regions by means of three receivers: RAD2 (13.825–1.075 MHz), RAD1 (1040–20 kHz), and TNR (256–4 kHz). For our purposes, we made use of data recorded by the RAD1 and TNR receivers. The kmTII events employed in this analysis were extracted from the Wind/WAVES Type II List at http://www-lep.gsfc.nasa.gov/waves, maintained by M. L. Kaiser. The list was examined for radio emissions occurring at frequencies <300 kHz, within the years 1997–2004. Altogether, 160 kmTII radio bursts were identified.

[8] To compare these events with the arrival of shocks at L1, we investigated shock catalogues from the Experimental Space Plasma Group at the University of New Hamp-

Table 1. Detail of the Total and Temporally Associated Number of Shocks and kmTII Events[a]

	Total Events	Temporally Associated Events	In UNH and MIT Lists	Only in UNH List	Only in MIT List	Only in WIND List
Shocks	296	99 (33%)	55	21+16	5	2
KmTIIs	160	92 (58%)				

[a]The last four columns list in addition the source of the identified shocks.

shire (hereinafter referred to as the UNH list, available at http://www-ssg.sr.unh.edu/mag/ace/ACElists/obs_list.html) and from the Space Plasma Group at the Massachusetts Institute of Technology (hereinafter referred to as the MIT list, available at http://space.mit.edu/home/jck/shockdb/shockdb.html). These lists enumerate shocks observed by the Advanced Composition Explorer (ACE) [*Stone et al.*, 1998], located near the L1 Lagrangian point.

[9] The above-mentioned lists were investigated for shocks detected by ACE within 3 days (72 hours) after the first appearance of a kmTII radio burst (note that a frequency of 300 kHz corresponds to a radial distance from the Sun of ~17 Rs or ~0.08 AU). Out of a total of 296 reported forward shocks (number based on the UNH list), 99 shocks (33%) were found in the vicinity of 92 kmTIIs (58% out of the total original number of 160; see columns 1 to 3 of Table 1). From these numbers, it is straightforward that there were some kmTIIs (7) temporally associated with more than one candidate shock. Figure 2 shows a yearly histogram of the 296 ACE forward shocks (light grey) and the 160 kmTIIs (dark grey) for comparison. The subset of ACE shocks in temporal agreement with any of the kmTIIs has been dotted, as has been also the subset of kmTIIs temporally associated with ACE shocks. The 68 resting kmTIIs not temporally associated with shocks near Earth may have either not been located near the Sun-Earth line or decayed to an MHD wave before striking the spacecraft.

[10] In general, the UNH ACE shock list was taken as a reference, and the MIT ACE shock list was consulted for verification. The detail of the contributions from each shock list is presented in columns 4–7 of Table 1. There were some few shock events (5) that were only listed in the MIT list. On the other hand, there were 21 shocks only listed in the UNH list (without taking into account the years 1997, 2003, and 2004, only available at the UNH list with 16 shocks). Fifty-five events were listed in both databases. During the survey process, if a kmTII resulted not to be in the vicinity of an ACE shock, also the Wind shock

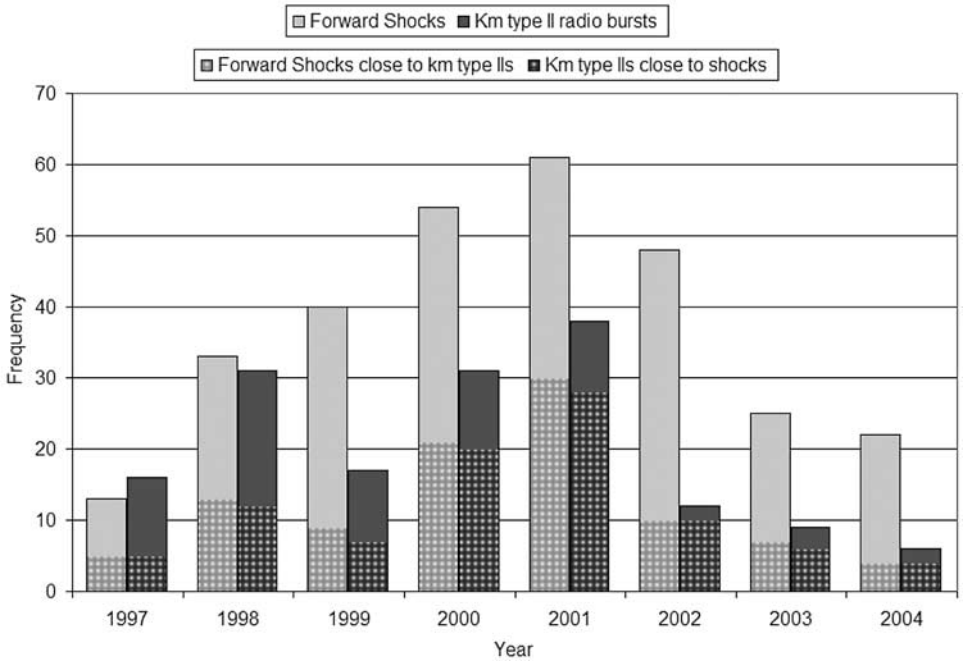

Figure 2. Yearly histogram of the 296 forward shocks seen by ACE, according to the UNH ACE shock list (light grey columns), in comparison with the 160 type II radio bursts extending through (or occurring in) the kilometric domain (dark grey columns). The number of ACE shocks found to be temporally associated with kilometric emissions has been dotted.

Table 2. The 99 Shock Events (Column 1), Their Temporally Associated Type II Radio Bursts in the Kilometric Domain (Columns 2–3), Frequency Range of the Sampled Radio Emissions (Columns 4–5), the Length, in Hours, of the Sampled Emission (Column 6), the Predicted Shock Arrival Time (Column 7), and the Resulting Error (Column 8)

Shock Arrival, UT	TII Radio Burst Start, UT	TII Radio Burst End, UT	Max Freq., kHz	Min Freq., kHz	Sampled Duration, hours	Predicted Shock Arrival Time, UT	Error, hours
09/21/1997 21:30	09/21/1997 02:00	09/21/1997 08:00	61	54	1.8	09/21/1997 21:42	0.2
11/01/1997 06:14[a]	10/31/1997 07:30	10/31/1997 12:30					
11/06/1997 22:02	11/04/1997 06:00	11/05/1997 04:30	252	197	1.7	11/06/1997 19:00	−3.0
11/09/1997 09:52	11/06/1997 12:20	11/07/1997 08:30	122	92	4.2	11/09/1997 10:13	0.2
11/22/1997 09:00[a]	11/19/1997 07:00	11/19/1997 14:00					
04/23/1998 17:28	04/23/1998 06:00	04/23/1998 15:30	127	88	3.1	04/24/1998 07:12	13.7
04/30/1998 08:43	04/28/1998 00:00	04/29/1998 00:00	69	61	5.2	05/02/1998 05:36	44.9[c]
05/01/1998 21:22	04/28/1998 00:00	04/29/1998 00:00	69	61	5.2	05/02/1998 05:36	8.3
05/03/1998 17:00	05/01/1998 12:00	05/03/1998 00:00	79	46	11.4	05/03/1998 05:04	−12.0
05/08/1998 03:21	05/07/1998 00:00	05/08/1998 00:00	102	73	5.5	05/09/1998 00:38	21.3
05/15/1998 13:57	05/14/1998 07:00	05/14/1998 22:00	83	74	6.7	05/19/1998 06:30	88.6[b]
06/17/1998 20:50	06/16/1998 18:20	06/17/1998 21:00	53	42	8.4	06/18/1998 23:30	26.7
08/26/1998 06:20	08/24/1998 22:05	08/26/1998 06:20	25	23	1.6	08/26/1998 07:06	0.4
09/24/1998 23:13	09/23/1998 07:20	09/24/1998 23:20	40	35	2.5	09/25/1998 00:42	1.4
10/02/1998 06:53	09/30/1998 13:20	10/02/1998 07:00	39	27	9.0	10/02/1998 01:24	−5.7
11/08/1998 04:21	11/05/1998 22:00	11/07/1998 08:00	70	51	10.0	11/08/1998 15:36	10.9
11/12/1998 06:31	11/11/1998 01:00	11/11/1998 18:00	73	62	4.1	11/13/1998 02:21	19.0
12/26/1998 09:30	12/23/1998 06:50	12/24/1998 15:00	162	135	3.1	12/27/1998 01:28	15.5
01/13/1999 10:00	01/11/1999 05:00	01/11/1999 21:00	71	46	15.4	01/13/1999 15:21	4.6
05/05/1999 14:59[a]	05/03/1999 05:50	05/03/1999 08:45					
05/05/1999 23:30[a]	05/03/1999 05:50	05/03/1999 08:45					
05/18/1999 00:03	05/13/1999 04:00	05/15/1999 04:00	185	114	8.5	05/17/1999 09:07	−15.4
07/02/1999 00:30	06/30/1999 23:00	07/01/1999 09:00	58	48	3.5	07/01/1999 23:18	−1.2
07/06/1999 14:20	07/03/1999 04:00	07/04/1999 12:00	54	40	7.4	07/06/1999 19:12	4.8
07/07/1999 07:00	07/05/1999 18:00	07/07/1999 00:00	89	48	16.4	07/08/1999 00:03	17.1[c]
07/08/1999 04:00	07/05/1999 18:00	07/07/1999 00:00	89	48	16.4	07/08/1999 00:03	−3.9
07/26/1999 23:33	07/26/1999 01:00	07/26/1999 16:00	46	31	4.7	07/27/1999 05:00	5.2
01/11/2000 13:40	01/09/2000 15:30	01/10/2000 12:00	199	134	3.9	01/12/2000 03:42	14.0
01/30/2000 18:44	01/29/2000 06:30	01/29/2000 16:00	94	56	8.4	01/30/2000 18:04	−0.7
02/11/2000 02:12	02/08/2000 09:05	02/11/2000 02:20	192	50	21.7	02/11/2000 02:54	0.3
02/11/2000 23:18	02/11/2000 08:45	02/11/2000 23:35	45	37	4.8	02/12/2000 03:31	4.0
02/20/2000 20:45[a]	02/17/2000 20:42	02/18/2000 22:12					
04/06/2000 16:04	04/05/2000 18:00	04/06/2000 16:00	109	42	10.1	04/06/2000 17:12	0.7
05/17/2000 21:35	05/15/2000 16:45	05/16/2000 14:00	65	52	2.7	05/17/2000 04:36	−17.0
06/08/2000 08:41	06/06/2000 15:20	06/08/2000 09:00	68	57	2.5	06/08/2000 06:24	−2.3
07/15/2000 14:15	07/14/2000 10:30	07/15/2000 14:30	173	62	7.0	07/15/2000 13:36	−0.7
07/19/2000 14:48	07/16/2000 03:00	07/16/2000 18:00	216	132	6.7	07/19/2000 21:14	5.7
07/28/2000 05:42	07/26/2000 09:30	07/27/2000 07:00	90	47	12.1	07/28/2000 04:44	−1.9
07/28/2000 09:09	07/26/2000 09:30	07/27/2000 07:00	90	47	12.1	07/28/2000 04:44	−4.5[c]
09/06/2000 16:13	09/05/2000 03:25	09/05/2000 11:25	40	28	6.0	09/06/2000 13:47	−2.4
09/15/2000 03:59	09/12/2000 12:00	09/13/2000 12:20	113	79	6.0	09/15/2000 06:38	2.2
10/03/2000 00:08	09/30/2000 13:00	10/01/2000 22:00	74	61	3.8	10/02/2000 22:18	−2.7
10/31/2000 16:30	10/29/2000 02:00	10/30/2000 18:00	91	70	7.8	10/31/2000 17:42	0.5
11/04/2000 01:34	11/01/2000 19:40	11/02/2000 13:00	40	36	4.1	11/03/2000 14:28	−12.0
11/11/2000 04:01	11/09/2000 16:15	11/11/2000 04:00	40	31	6.9	11/10/2000 21:46	−6.4
11/19/2000 01:43	11/17/2000 00:00	11/17/2000 16:00	218	167	3.9	11/21/2000 11:08	57.4
11/26/2000 05:00	11/24/2000 05:10	11/24/2000 15:00	465	151	4.9	11/26/2000 03:06	−2.4
11/26/2000 11:24	11/24/2000 15:25	11/24/2000 22:00	399	217	3.0	11/27/2000 02:46	15.0
01/10/2001 15:19	01/06/2001 22:00	01/07/2001 10:00	65	61	3.8	01/11/2001 05:42	13.5[b]
01/13/2001 01:42	01/12/2001 03:30	01/13/2001 10:00	20	18.5	3.3	01/12/2001 23:12	−3.2
01/17/2001 15:31	01/14/2001 20:30	01/15/2001 11:00	342	284	1.0	01/17/2001 20:42	4.3
01/31/2001 07:22	01/28/2001 15:45	01/28/2001 17:00	173	143	1.3	01/30/2001 13:52	−18.7
03/30/2001 21:51	03/29/2001 10:12	03/30/2001 06:00	180	114	2.1	03/30/2001 18:06	−3.7
03/31/2001 00:23	03/29/2001 10:12	03/30/2001 06:00	180	114	2.1	03/30/2001 18:06	−6.3[c]
04/07/2001 16:59	04/06/2001 19:35	04/07/2001 17:00	70	44	5.8	04/07/2001 23:18	5.4
04/08/2001 16:59	04/06/2001 19:35	04/07/2001 17:00	70	44	5.8	04/07/2001 23:18	−12[c]
04/11/2001 13:14	04/09/2001 15:53	04/10/2001 01:00	134	106	2.2	04/11/2001 11:46	−2.4
04/11/2001 15:27	04/10/2001 05:24	04/11/2001 00:00	197	147	1.3	04/11/2001 12:06	−4.2
04/18/2001 00:04	04/15/2001 14:05	04/16/2001 13:00	59	47	3.9	04/18/2001 05:46	5.0
04/28/2001 04:31	04/26/2001 12:40	04/28/2001 05:00	38	24	9.1	04/27/2001 20:06	−8.9
05/06/2001 07:06	05/04/2001 06:00	05/05/2001 14:00	110	91	3.6	05/06/2001 18:58	9.9
06/18/2001 01:54	06/15/2001 06:45	06/15/2001 10:00	91	67	2.8	06/16/2001 04:41	−45.4
08/12/2001 10:48	08/10/2001 01:00	08/10/2001 22:00	69	35	11.3	08/11/2001 07:54	−27.3

Table 2. (continued)

Shock Arrival, UT	TII Radio Burst Start, UT	TII Radio Burst End, UT	Max Freq., kHz	Min Freq., kHz	Sampled Duration, hours	Predicted Shock Arrival Time, UT	Error, hours
08/17/2001 10:16	08/16/2001 00:10	08/16/2001 20:00	53	47	1.3	08/17/2001 06:55	−4.1
08/27/2001 19:19	08/25/2001 16:50	08/25/2001 23:00	71	51	6.1	08/27/2001 11:34	−8.1
09/13/2001 02:31	09/12/2001 10:00	09/12/2001 22:00	57	38	6.7	09/13/2001 06:11	3.7
09/14/2001 01:17	09/13/2001 17:40	09/14/2001 05:45	89	57	8.9	09/15/2001 13:33	35.6
09/25/2001 20:05	09/24/2001 10:45	09/25/2001 20:00	30.5	29	2.2	09/25/2001 14:38	−5.6
09/29/2001 09:06	09/27/2001 08:15	09/28/2001 07:00	629	420	0.8	09/29/2001 11:43	2.2
10/03/2001 08:06	10/01/2001 07:00	10/01/2001 18:30	250	133	3.6	10/03/2001 00:55	−7.2
10/11/2001 16:19	10/09/2001 13:10	10/10/2001 23:00	47	38	7.4	10/11/2001 17:28	0.6
10/21/2001 16:12	10/19/2001 16:45	10/21/2001 16:40	84	59	4.9	10/21/2001 12:01	−4.7
10/28/2001 02:41	10/25/2001 15:30	10/27/2001 23:00	65	56	2.7	10/28/2001 05:45	2.5
10/31/2001 12:53	10/28/2001 14:00	10/30/2001 00:00	376	215	9.2	10/06/2001 05:00	111.2[b]
11/06/2001 01:25	11/04/2001 16:30	11/06/2001 11:00	255	155	3.6	11/07/2001 04:18	26.9
11/19/2001 17:35	11/17/2001 17:00	11/18/2001 03:30	141	87	5.4	11/19/2001 13:22	−4.9
11/24/2001 05:45	11/22/2001 20:50	11/24/2001 02:30	64	44	4.9	11/24/2001 02:24	−3.5
12/29/2001 04:47	12/26/2001 05:20	12/27/2001 05:00	541	197	5.6	12/29/2001 05:54	0.6
01/10/2002 15:44	01/08/2002 18:30	01/10/2002 00:00	235	95	7.1	01/10/2002 17:51	2.1
01/17/2002 05:44	01/14/2002 06:25	01/14/2002 21:30	552	260	2.5	01/16/2002 09:23	−20.3
02/17/2002 02:09	02/14/2002 00:10	02/14/2002 13:50	139	112	6.8	02/19/2002 21:00	67.6[b]
04/19/2002 08:02	04/17/2002 08:30	04/19/2002 04:00	32	27	7.6	04/18/2002 23:18	−9.1
04/23/2002 04:15	04/21/2002 01:30	04/22/2002 00:00	92	60	6.4	04/22/2002 23:47	−5.2
05/23/2002 10:15	05/22/2002 04:10	05/23/2002 10:40	41	37	1.6	05/23/2002 09:16	−1.5
07/17/2002 15:26	07/15/2002 21:15	07/16/2002 05:00	271	127	4.7	07/17/2002 19:47	3.9
08/18/2002 18:10	08/16/2002 12:20	08/17/2002 21:00	81	55	6.0	08/18/2002 19:34	0.9
09/07/2002 16:08	09/05/2002 16:55	09/07/2002 16:22	42	32	3.6	09/07/2002 15:53	−0.5
11/11/2002 11:52	11/09/2002 13:20	11/10/2002 03:00	238	136	3.6	11/11/2002 09:58	−1.9
05/29/2003 18:25	05/28/2003 01:00	05/29/2003 00:30	127	76	5.5	05/29/2003 22:04	3.6
05/30/2003 16:00	05/29/2003 01:10	05/29/2003 08:00	833	223	2.8	05/30/2003 14:03	−2.0
06/18/2003 14:40	06/17/2003 22:50	06/18/2003 05:30	314	128	6.8	06/20/2003 11:41	45[c]
06/20/2003 08:00	06/17/2003 22:50	06/18/2003 05:30	314	128	6.8	06/20/2003 11:41	3.7
10/30/2003 16:19	10/28/2003 11:10	10/30/2003 00:00	54	38	11.7	10/30/2003 07:54	−8.4
11/04/2003 05:59	11/02/2003 17:30	11/03/2003 01:00	61	53	1.8	11/03/2003 19:58	−10.8
11/06/2003 19:19	11/04/2003 20:00	11/05/2003 00:00	348	242	1.4	11/06/2003 18:43	−0.6
07/26/2004 22:30	07/25/2004 15:00	07/26/2004 22:25	75	49	5.1	07/26/2004 20:51	−1.6
09/13/2004 19:40	09/12/2004 00:45	09/13/2004 21:00	74	55	3.7	09/13/2004 20:23	0.7
11/09/2004 09:10	11/07/2004 16:25	11/08/2004 20:00	79	63	3.8	11/09/2004 14:13	4.8
12/05/2004 07:00	12/02/2004 00:07	12/04/2004 04:30	88	62	6.0	12/05/2004 00:30	−6.5

[a]Events which could not be fitted because the emission was too chaotic or reduced to a single spot.
[b]Events discarded because their speed was implausibly slow (below 300 km s^{-1}).
[c]Events which were superseded by a second candidate which yielded closer predictions.

list at MIT was consulted. Only 2 kmTIIs not temporally associated with any ACE shock were found to be with Wind shocks.

[11] The 99 shocks identified in the vicinity of 92 type II radio emissions extending to/occurring in the kilometric domain have been listed in column 1 of Table 2. Start and end time of the temporally associated type II radio bursts, as well as their sampled frequency range, are given in columns 2–5. The remaining columns will be addressed in section 4.

3. Analysis Technique

[12] The prediction method relies on the detection of emission from electrons as a shock travels through the interplanetary medium. The emission, occurring at the local plasma frequency (f) or its harmonic, is directly related to the local electron density by $n_e = (f/9)^2$. If one then assumes a coronal/interplanetary model of electron density, it is possible to obtain an estimate of the distance from the Sun at which the radio emission is occurring. The Leblanc model [*Leblanc et al.*, 1998], used for this study, is derived from Wind/WAVES and ground-based radio observations. It assumes an electron density at 1 AU of $n_0 = 7.2$ cm^{-3}, though it can be adjusted for other densities.

[13] The slope of the drifting radio emission was calculated for all of the kmTII radio bursts found to be in temporal association with shocks detected in situ. We "associated" a kmTII event with a shock if the latter was detected within 3 days (72 hours) after the first appearance of the radio emission. We chose to examine the data points from dynamic spectral plots in the 1/f space, as graphed in Figure 1, where the slowly drifting radio emissions are organized along a straight line, since 1/f can be assumed to be equivalent to the heliocentric distance R [*Bougeret et al.*, 1984; *Reiner et al.*, 1998b]. If most of the deceleration has occurred near the Sun, then $R \approx v\,(t - t_0)$, where v is the shock speed, t is the time, and t_0 is the onset time. It follows that the shock speed can be estimated from the drift rate through the expression $v = \text{slope}*a*R_0*\sqrt{n_0}$

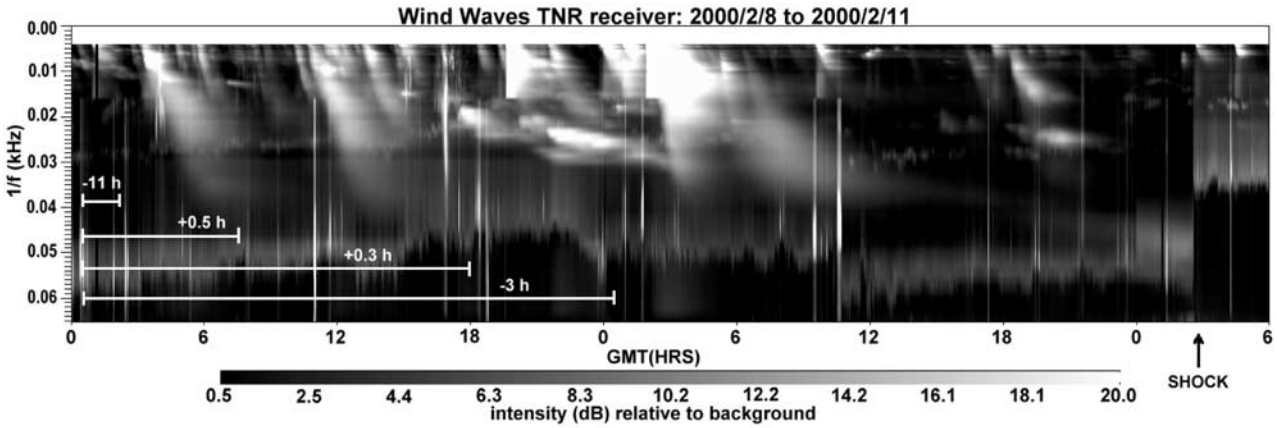

Figure 3. Dynamic spectrum of a kilometric type II radio burst registered by the TNR receiver on 8 February 2000. Note the scale of the vertical axis is in units of 1/f. It took more than 2 days for the radio emission produced by this CME-driven shock to reach the Wind spacecraft at 0212 UT on 11 February 2000. The horizontal lines indicate the segment of kmTII used to calculate the drift rate, while the numbers above them indicate the corresponding resulting error.

[*Reiner et al.*, 1998b], where a = 9 or 18 if the emission occurs at the fundamental or the harmonic of the plasma frequency, respectively, and $R_0 = 1.5 \times 10^8$ km. It is assumed in this study that the emission is generated along the Sun-Earth line, so that R lies always between the Sun and the Earth. By knowing the shock speed and the distance R at which the radio emission is generated (derived from the Leblanc model), the predicted shock arrival time is ultimately obtained. We then define an ''error'' as given by the difference between the predicted and the real arrival time. Thus a negative error indicates an underestimation of the shock arrival time, i.e., the shock arrived after it was expected to and vice versa. The shock time at Wind, extracted from the Wind shock list at MIT, was taken as the real shock arrival time. The TNR receiver also sees sudden increases in the local plasma frequency which are usually (but not always) due to shocks. At times when the complicated orbit of Wind constrains the spacecraft to be outside Earth's magnetosphere, the ACE shock time was taken into account.

[14] All the bursts analyzed here extend down to kilometric wavelengths (300–30 kHz). In some cases it was less ambiguous to measure them at higher frequencies; therefore the frequency range is more accurately called ''hectometric/kilometric.'' Further, it is worth to note that these emissions are a subset of the so-called IP type II events, usually broad bands that start below 4 MHz [see *Cane et al.*, 1982].

[15] An example is presented in Figure 3. This event is somewhat fragmented but at the same time its drift rate can be measured multiple times over more than 48 hours prior to the shock arrival. The patchy structure is fairly typical of the events measured in this study, although it is not common that these intermittent emissions persist for more than 2 days, as in this example. The worst prediction, as defined by the ''error,'' arises from the shortest interval measured. As the extension of the measured segment is increased, the prediction improves. However, changes in the properties of the interplanetary medium and in the unsteady solar wind plasma frequency line may cause the prediction to deviate away from the real shock arrival time. Another issue is to determine whether the observed emission is occurring at the fundamental or the harmonic plasma frequency. If both are present (35 cases), or if the obtained shock speed is illogical (24 cases), the decision is straightforward. Otherwise, the valuable expertise from the forecaster allows him to decide based on the best educated guess. Overall, the nature of the emission was unclear for 25 kmTIIs.

4. Results and Discussion

[16] The actual shock arrival times as received by the Wind spacecraft were subtracted from the predicted ones calculated according to the technique presented in the previous section. The resulting difference between these shock arrival times (the error) is displayed in Figure 4, in a histogram in consecutively duplicating bins. In the figure, a total of 84 events have been plotted in a histogram after refining the data set: from the starting 92 events, four were discarded because their estimated speed resulted implausibly slow (less than 300 km s^{-1}, probably a corotating shock associated with a CIR; denoted with a superscript *b* in Table 2), while for five other radio events, the drift rate could not be calculated either because the emission was too chaotic or reduced to a single spot (indicated with a superscript *a* in Table 2). In addition, it is worth to note that for seven radio events, there was more than one candidate shock temporally associated (superscript *c*). In

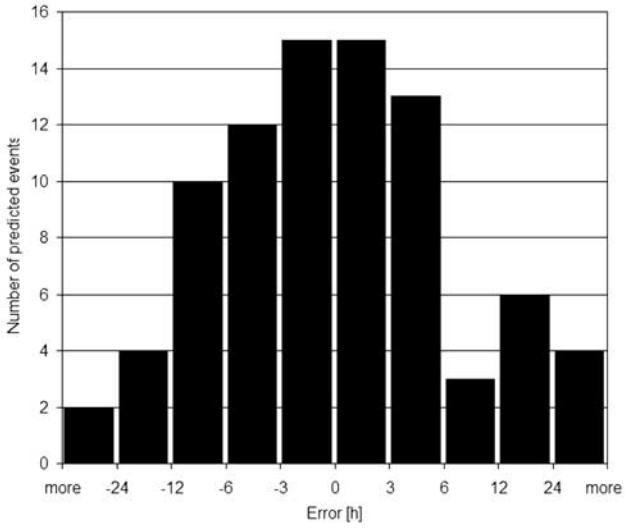

Figure 4. Histogram of the error in predicted shock arrival times, in consecutively duplicating bins. A negative value of the error indicates an underestimation of the real shock arrival time, while a positive one denotes an overestimation.

those cases, the shock that was taken into account was that one whose arrival time approximated best the predicted one.

[17] The resulting histogram in Figure 4 indicates that 55 (66%) of the analyzed kmTIIs yielded predicted shock arrival times ±6 hours within the real one. The average error for this subset of events is 2.7 hours, while the overall average error is 8 hours. Only six events (7%) were forecast with errors larger than 24 hours, out of which three could have been predicted with smaller than 24 hours errors if the harmonic/fundamental "best guess" decision would have been the correct one. From the inspection of column 5 of Table 2, it can be noted that all those events whose sampled frequency extended below 50 kHz (but two, i.e., 32 events or 38% of the sample) allowed the prediction of a shock within 12 hours of the real shock arrival time. For higher values of minimum sampled frequency, larger values of the error are more frequent.

[18] These results show significant improvement over the previous ones obtained from metric type II radio bursts [*McKenna-Lawlor et al.*, 2002; *Cho et al.*, 2003; *Smith et al.*, 2003; *Fry et al.*, 2003; *McKenna-Lawlor et al.*, 2006]. The latter two studies present predictions for 68 and 55 shocks, respectively, calculated on the basis of the STOA, ISPM, and HAFv.2 models. Together, those 123 shocks are spread over the period February 1997 to August 2002. The comparison of the events presented in this study with those analyzed by *Fry et al.* [2003] and *McKenna-Lawlor et al.* [2006] yielded 47 shocks in common. In Figure 5, the errors of the shock arrival times as derived from the STOA, ISPM, and HAFv.2 models (vertical axis) are contrasted with the errors obtained with the kmTII technique (horizontal axis). The three series show similar, near-symmetrical distributions, though ISPM appears somewhat biased toward negative values. The most prominent difference between metric Type II-derived shock arrival times and kmTII-derived ones is that the former are essentially spread within the range −30 to 15 hours, while the latter are mostly concentrated within ±6 hours. The technique employed to calculate shock arrival times based on kilometric radio emissions proves to be considerably more accurate, allowing the prediction of 2/3 of the events with a mean error smaller than 6 hours.

[19] The values of transit speed derived by means of the described method are compared to the corresponding in situ speeds in Figure 6. The latter ones were mainly obtained from the Wind shock list at MIT, except for those events where the shock was only seen by ACE, in which case the values of speed ACE shock list at MIT was consulted. Both of these lists obtain the key shock parameters by means of eight different techniques: the value of speed used for the comparison in Figure 6 is the median of those. From the plot in Figure 6, it is straightforward that the transit speeds deduced from the kmTII radio bursts result to be higher than the corresponding in situ speeds. That is, the shock producing the kmTII was moving always faster than when it arrived at Earth, in rough average by a factor of 1.25. Further deceleration and the characteristics of the emission mechanism may play a role in this discrepancy. Similar discrepancies were found by, e.g., *Dal Lago et al.* [2004, Figure 2].

[20] It is of interest to find the main factors that influence the error. In an effort to do so, the error has been plotted as a function of the time remaining to the real shock arrival (see Figure 7). The length of the horizontal stripes represents the length (in hours) of the kmTII emission measured to calculate the shock arrival time. It would be expected, that the farther the radio emission is from the spacecraft, the larger the errors when producing the forecast. Moreover, a short sampled radio emission is presumed to yield imprecise predictions. However, Figure 7 does not confirm the expected: short-sampled, far from

Figure 5. Errors in shock arrival time derived from metric Type II radio bursts (vertical axis) versus errors in shock arrival time derived from the technique here presented, based on kmTII radio emissions (horizontal axis). The three data series correspond to the three methods utilized to calculate shock arrival times from metric Type II radio bursts in the work of *Fry et al.* [2003] and *McKenna-Lawlor et al.* [2006]. The errors in shock arrival time derived from kmTII radio bursts are mostly concentrated within ±6 hours, while errors derived from other techniques are spread within −30 hours to 15 hours.

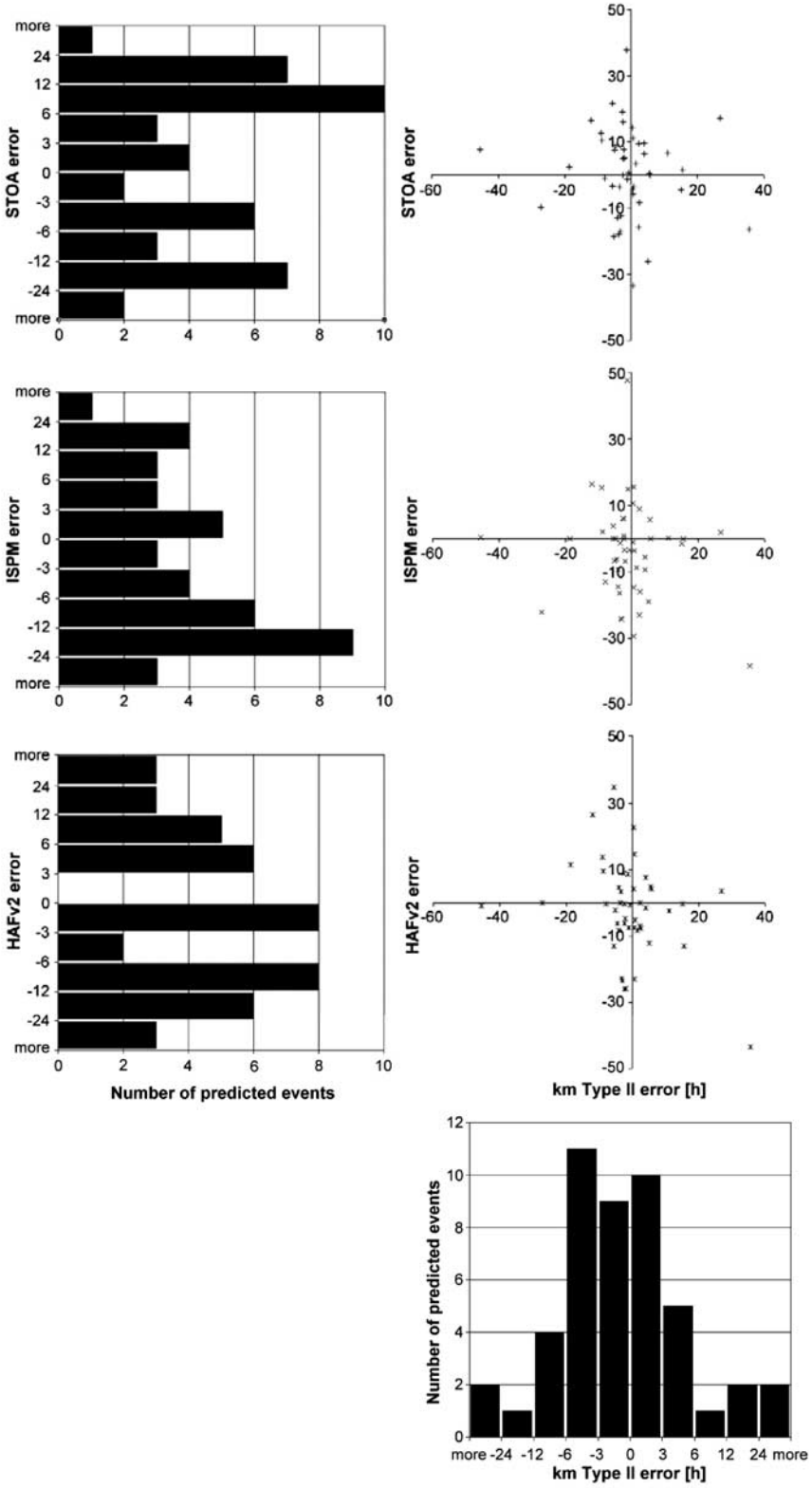
STOA error
ISPM error
HAFv2 error
more
24
12
6
3
0
-3
-6
-12
-24
more
0 2 4 6 8 10
Number of predicted events
50
30
10
-10
-30
-50
-60 -40 -20 20 40
km Type II error [h]
Number of predicted events
12
10
8
6
4
2
0
more -24 -12 -6 -3 0 3 6 12 24 more
km Type II error [h]

Figure 5

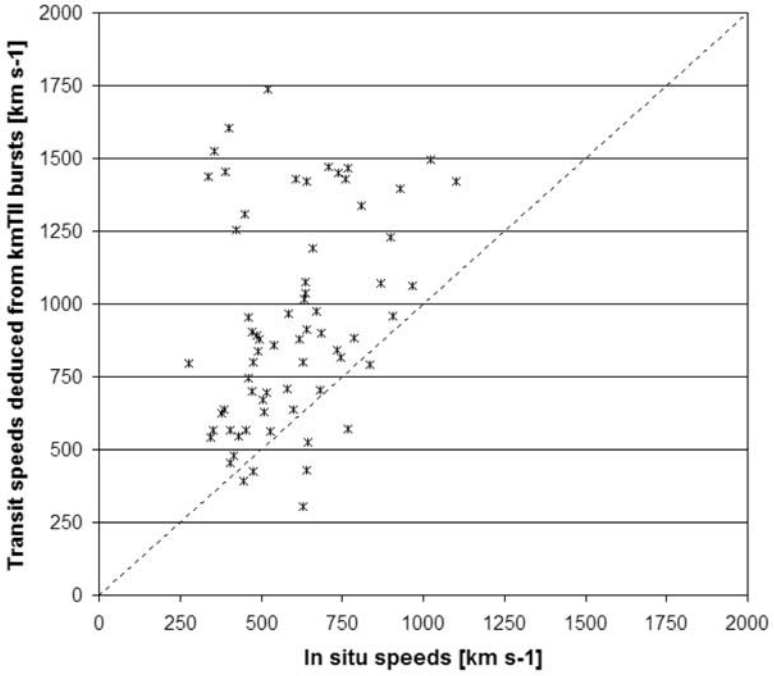

Figure 6. Transit speeds deduced from the analyzed kmTII radio bursts versus speeds deduced from in situ measurements. The latter values correspond to the median of the values of speed deduced by J. Kasper at the MIT lists.

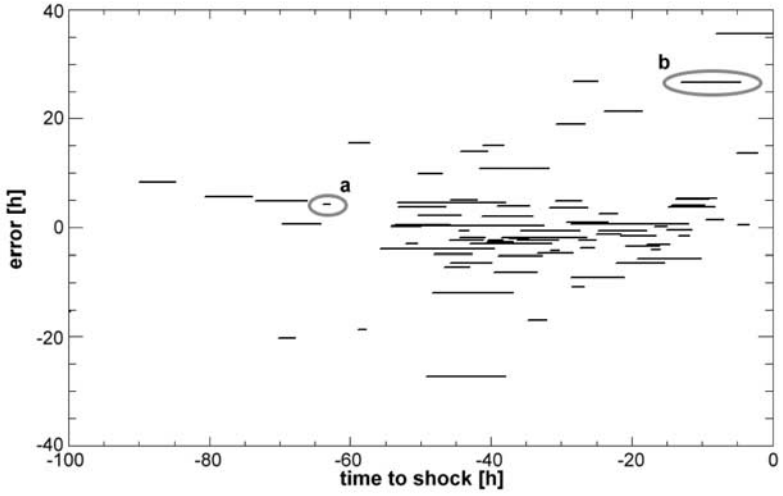

Figure 7. Error versus remaining time to real shock arrival, in hours. The length of the horizontal stripes indicates, in hours, the duration of the sampled measured radio emission. Two extreme cases have been encircled. The circle marked with a bold ''a'' is a short-sampled kmTII and also far from the real shock arrival time but which yielded a very small error, while the circle marked with a bold ''b'' is a kmTII measured for over 10 hours and quite close to the real shock arrival time, which yielded a very poor prediction.

Table 3. Number of Shocks That Would Have Been Predicted 24 Hours Before Their Arrival and 12 Hours Before Their Arrival As Well As the Fraction That Would Have Been Successfully Predicted Within a Hit Window of ±24 Hours and ±12 Hours, Respectively

	Min. Forecast Time = 24 Hours	Min Forecast Time = 12 Hours
All predictions	61 (73%)	80 (95%)
Only hits, hit window = ±24 hours	56 (67%)	74 (88%)
Only hits, hit window = ±12 hours	47 (56%)	62 (74%)

the shock kmTIIs as the example denoted ***a***, may provide good predictions, while long-sampled emissions very close to the shock arrival time as ***b*** may give quite erroneous results. Distance from the shock and the temporal length of the measured kmTII seem not to substantially affect the quality of the prediction. As shown above in Figure 3, a radio emission measured over a long period of time will not necessarily improve the predictions. Actually, the principal cause of error (in the case that shock and kmTII are in fact associated) seems to be the fluctuation of the plasma frequency at the site of the spacecraft. In specific cases, the nominal value for n_0 = 7.2 cm^{-3} was replaced for a more realistic one. That was possible for 14 events, out of which 11 occurred during solar minimum, when the electron frequency at 1 AU had stable values but different from the usually assumed 7.2 cm^{-3}. These ranged from 1.5 to 9.7 cm^{-3}, yielding successful predictions within ±24 hours (±12 hours) in 12 (10) cases and unsuccessful in two (four). The replacement of n_0 for more proper values in the Leblanc model yielded good results and proved to be useful in improving the shock arrival predictions. Nevertheless, in times of solar maximum, the highly fluctuating solar wind hinders the stability of n_0, making it impossible to approximate it to a better value other than 7.2 cm^{-3}. Errors in the estimation of the shock arrival time could be partially accounted by the failure to predict the rms value of n_0 at Earth. According to *Leblanc et al.* [1998], the rms value of n_0 ranges overall from 2 to 39 cm^{-3} and essentially from 3 to 12 cm^{-3}. The latter range would imply errors in the shock arrival time prediction of ~7 hours to ~15 hours for harmonic and of ~15 hours to ~40 hours for fundamental emissions. These numbers are somewhat far from the "bulk" of the errors resulting from the predictions derived from the kmTIIs and presented in Figure 4, since 2/3 of the events could be predicted with a mean error smaller than 6 hours. However, it is highly likely that the errors result, at least partially, from fluctuations of the solar wind density at Earth.

[21] A potential restriction in the presented technique is the proximity of the employed kmTII radio emissions to Earth. In certain cases, the kilometric type II radio bursts are not observed until within a day of the detection of a shock at L1. Depending on the application of the forecast, a specific minimum period of time will be required to issue the predictions. In order to consider this factor, Table 3 has been put together. If the minimum forecast time required is assumed to be of 24 hours (column 1 of Table 3), 61 (73%) of the 84 analyzed events would be forecasted early enough to announce the warnings, out of which 56 would have successfully predicted shock arrival times within ±24 hours and 47 within ±12 hours. Moreover, if the minimum forecast time limit is reduced to 12 hours (column 2 of Table 3), 80 (95%) of the shock events would be timely forecasted, out of which 74 would have been successfully predicted within ±24 hours and 62 within ±12 hours.

[22] The analysis of low-frequency radio emissions, as presented in this article, shows a great potential toward improved predictions of shock arrival. Even if only 33% of the ACE forward shocks were temporally associated with kmTII emissions, the presence of one implies the possibility of substantial improvement of the forecast. Future prospects of this technique include linking kmTII emissions with their counterparts close to the Sun, so as to reduce false alarms given by events not located on the Sun-Earth line. The possibility that LASCO and/or SECCHI speeds of the associated CMEs may contribute to improve the presented technique will also be evaluated.

[23] The proposed method has the likely disadvantage that it relies on radio measurements in the kilometric domain, only possible from space. The continuity of missions that perform measurements at these frequencies is crucial for the proposed technique.

[24] **Acknowledgments.** The WAVES experiment on the Wind spacecraft is a joint project of the Observatoire de Paris, NASA/GSFC and the University of Minnesota. The shock lists employed in this study are maintained by Charles W. Smith at the University of New Hampshire and Justin C. Kasper at the Massachusetts Institute of Technology. The authors would like to thank Ernesto Aguilar-Rodriguez for providing the tool employed to obtain information on data points of WAVES plots, Adam Szabo for his help on existing shock databases, and Nat Gopalswamy for useful discussions.

References

Bougeret, J.-L., J. H. King, and R. Schwenn (1984), Solar radio burst and in situ determination of interplanetary electron density, *Sol. Phys.*, *90*, 401–412.

Bougeret, J.-L., M. L. Kaiser, P. J. Kellogg, R. Manning, K. Goetz, S. J. Monson, N. Monge, L. Friel, C. A. Meetre, C. Perche, L. Sitruk, and S. Hoang (1995), Waves: The Radio and Plasma Wave Investigation on the Wind Spacecraft, *Space Sci. Rev.*, *71*, 231–263.

Bougeret, J.-L., et al. (2007), STEREO/WAVES: Interplanetary radio burst tracker, *Space Sci. Rev.*, in press.

Cane, H. V., and W. C. Erickson (2005), Solar Type II radio bursts and IP Type II events, *Astrophys. J.*, *623*, 1180–1194.

Cane, H. V., R. G. Stone, J. Fainberg, J. L. Steinberg, and S. Hoang (1982), Type II solar radio events observed in the interplanetary medium, *Sol. Phys.*, *78*, 187–198.

Cane, H. V., N. R. Sheeley Jr., and R. A. Howard (1987), Energetic interplanetary shocks, radio emission, and coronal mass ejections, *J. Geophys. Res.*, *92*, 9869–9874.

Cho, K. S., Y.-J. Moon, M. Dryer, C. D. Fry, Y.-D. Park, and K.-S. Kim (2003), A statistical comparison of interplanetary shock and CME propagation models, *J. Geophys. Res.*, *108*(A12), 1445, doi:10.1029/2003JA010029.

Claßen, H. T., and H. Aurass (2002), On the association between Type II radio bursts and CMEs, *Astron. Astrophys.*, *384*, 1098–1106, doi:10.1051/0004-6361:20020092.

Dal Lago, A., L. E. A. Vieira, E. Echer, W. D. Gonzalez, A. L. C. de Gonzalez, F. L. Guarnieri, N. J. Schuch, and R. Schwenn (2004), Comparison between halo CME expansion speeds observe don the Sun, the related shock transit speeds to Earth, and corresponding ejecta speeds at 1 AU, *Sol. Phys.*, *222*, 323–328.

Dryer, M., and D. F. Smart (1984), Dynamical models of coronal transients and interplanetary disturbances, *Adv. Space Res.*, *4*, 291–301.

Dulk, G. A., Y. Leblanc, and J.-L. Bougeret (1999), Type II shock and CME from the corona to 1 AU, *Geophys. Res. Lett.*, *26*(15), 2331–2334.

Fry, C. D., W. Sun, C. S. Deehr, M. Dryer, Z. Smith, S.-I. Akasofu, M. Tokumaru, and M. Kojima (2001), Improvements to the HAF solar wind model for space weather predictions, *J. Geophys. Res.*, *106*(A10), 20,985–21,001.

Fry, C. D., M. Dryer, Z. Smith, W. Sun, C. S. Deehr, and S.-I. Akasofu (2003), Forecasting solar wind structures and shock arrival times using an ensemble of models, *J. Geophys. Res.*, *108*(A2), 1070, doi:10.1029/2002JA009474.

Gary, D. E., G. A. Dulk, L. House, R. Illing, C. Sawyer, W. J. Wagner, D. J. McLean, and E. Hildner (1984), Type II bursts, shock waves, and coronal transients: The event of 1980 June, 29, 0233 UT, *Astron. Astrophys.*, *134*, 222–233.

Gopalswamy, N., A. Lara, M. L. Kaiser, and J.-L. Bougeret (2001a), Near-Sun and near-Earth manifestations of solar eruptions, *J. Geophys. Res.*, *106*(A11), 25,261–25,277.

Gopalswamy, N., A. Lara, S. Yashiro, M. L. Kaiser, and R. A. Howard (2001b), Predicting the 1-AU arrival of coronal mass ejections, *J. Geophys. Res.*, *106*(A12), 29,207–29,218.

Howard, T. A., D. F. Webb, S. J. Tappin, D. R. Mizuno, and J. C. Johnston (2006), Tracking halo coronal mass ejections from 0–1 AU and space weather forecasting using the Solar Mass Ejection Imager (SMEI), *J. Geophys. Res.*, *111*, A04105, doi:10.1029/2005JA011349.

Howard, R. A., et al. (2007), Sun Earth Connection Coronal and Heliospheric Investigation (SECCHI), *Space Sci. Rev.*, in press.

Leblanc, Y., G. A. Dulk, and J.-L. Bougeret (1998), Tracing the electron density from the corona to 1 AU, *Sol. Phys.*, *183*, 165–180.

Leblanc, Y., G. A. Dulk, A. Vourlidas, and J.-L. Bougeret (2001), Tracing shock waves from the corona to 1 AU: Type II radio emission and relationship with CMEs, *J. Geophys. Res.*, *106*(A11), 25,301–25,312.

Manoharan, P. K. (2006), Evolution of coronal mass ejections in the inner heliosphere: A study using white light and scintillation images, *Sol. Phys.*, *235*, 345–368.

Mays, M. L., O. C. St. Cyr, E. Quémerais, S. Ferron, J.-L. Bertaux, S. Yashiro, and R. Howard (2007), An attempt to detect coronal mass ejections in Lyman-α using SOHO SWAN, *Sol. Phys.*, *241*, 113–125.

McKenna-Lawlor, S. M. P., M. Dryer, Z. Smith, K. Kecskemety, C. D. Fry, W. Sun, C. S. Deehr, D. Berdichevsky, K. Kudela, and G. Zastenker (2002), Arrival times of Flare/Halo CME associated shocks at Earth: comparison of the predictions of three numerical models with these observations, *Ann. Geophys.*, *20*, 917–935.

McKenna-Lawlor, S. M. P., M. Dryer, M. D. Kartalev, Z. Smith, C. D. Fry, W. Sun, C. S. Deehr, K. Kecskemety, and K. Kudela (2006), Near real-time predictions of the arrival at Earth of flare-related shocks during Solar Cycle 23, *J. Geophys. Res.*, *111*, A11103, doi:10.1029/2005JA011162.

Pick, M. (1999), Radio and coronagraph observations: shocks, coronal mass ejections and particle acceleration, in *Proceedings of the Nobeyama Symposium*, *NRO Rep. 479*, edited by T. S. Bastian, N. Gopalswamy, and K. Shibasaki, pp. 187–198, Nobeyama Radio Obs., Nagano, Japan.

Reiner, M. J., M. L. Kaiser, J. Fainberg, J.-L. Bougeret, and R. G. Stone (1998a), On the origin of radio emissions associated with the January 6–11, 1997, CME, *Geophys. Res. Lett.*, *25*(14), 2493–2496.

Reiner, M. J., M. L. Kaiser, J. Fainberg, and R. G. Stone (1998b), A new method for studying remote type II radio emissions from coronal mass ejection-driven shocks, *J. Geophys. Res.*, *103*(A12), 29,651–29,664.

Schwenn, R., A. Dal Lago, W. D. Gonzalez, E. Huttunen, O. C. St. Cyr, and S. P. Plunkett (2001), A tool for improved space weather predictions: The CME expansion speed, *Eos Trans. AGU*, *82*, 47.

Sheeley, N. R., Jr., R. A. Howard, D. J. Michels, M. J. Koomen, R. Schwenn, K. H. Muehlhaeuser, and H. Rosenbauer (1985), Coronal mass ejections and interplanetary shocks, *J. Geophys. Res.*, *90*, 163–175.

Smith, Z., and M. Dryer (1995), The Interplanetary Shock Propagation Model: A model for predicting solar-flare-caused geomagnetic sudden impulses based on the 2 1/2 D MHD numerical simulation results from the Interplanetary Global Model (2D IGM), *Tech. Memo. ERL/SEL-89*, NOAA, Washington, D. C.

Smith, Z., W. Murtagh, T. Detman, M. Dryer, C. D. Fry, and C.-C. Wu (2003), Study of solar-based inputs into space weather models that predict interplanetary shock arrivals at Earth, in *Proceedings of ISCS 2003 Symposium "Solar Variability as an Input to the Earth's Environment,"* edited by A. Wilson, pp. 547–552, Eur. Space Agency, Noordwijk, Netherlands.

Stone, E. C., A. M. Frandsen, R. A. Mewaldt, E. R. Christian, D. Margolies, J. F. Ormes, and F. Snow (1998), The Advanced Composition Explorer, *Space Sci. Rev.*, *86*(1/4), 1–22.

H. Cremades and O. C. St. Cyr, NASA Goddard Space Flight Center, Code 670, Greenbelt, MD 20771, USA. (cremades@helio.gsfc.nasa.gov)

M. L. Kaiser, NASA Goddard Space Flight Center, Code 695, Greenbelt, MD 20771, USA.